Journal of
Materials Chemistry A

Accepted Manuscript

This is an *Accepted Manuscript*, which has been through the RSC Publishing peer review process and has been accepted for publication.

Accepted Manuscripts are published online shortly after acceptance, which is prior to technical editing, formatting and proof reading. This free service from RSC Publishing allows authors to make their results available to the community, in citable form, before publication of the edited article. This *Accepted Manuscript* will be replaced by the edited and formatted *Advance Article* as soon as this is available.

To cite this manuscript please use its permanent Digital Object Identifier (DOI®), which is identical for all formats of publication.

More information about *Accepted Manuscripts* can be found in the **Information for Authors**.

Please note that technical editing may introduce minor changes to the text and/or graphics contained in the manuscript submitted by the author(s) which may alter content, and that the standard **Terms & Conditions** and the **ethical guidelines** that apply to the journal are still applicable. In no event shall the RSC be held responsible for any errors or omissions in these *Accepted Manuscript* manuscripts or any consequences arising from the use of any information contained in them.

ARTICLE Journal Name

Incapsulation of γ-Fe_2O_3 decorated reduced graphene oxide in polyaniline core-shell tubes as an exceptional tracker for electromagnetic environmental pollution

Cite this: DOI: 10.1039/x0xx00000x

Received 00th January 2012,
Accepted 00th January 2012

DOI: 10.1039/x0xx00000x

www.rsc.org/

Avanish Pratap Singh[a,d], Monika Mishra[a], Pradeep Sambyal[a], Bipin Kumar Gupta[b], Bhanu Pratap Singh[c], Amita Chandra[d] and S. K. Dhawan[a*]

The ultimate goal of development of a new material γ-Fe_2O_3 decorated reduced graphene oxide (rGO):Polyaniline (PANI) core-shell tubes has been done for absorbing electromagnetic interference (EMI) pollution. Herein, we report the synthesis and characterization of a PANI tubes consisting of rGO decorated with iron oxide nanoparticles (RF). The intercalated RF was synthesized by thermal decomposition of ferric acetyl acetonate in reducing atmosphere. Furthermore, RF was further encapsulated through the oxidative polymerization of aniline in the presence of β–Naphthalene sulphonic acid which results in RF/PANI core-shell morphology. Scanning electron microscopy results confirm the formation of tubular core-shell morphology having 5-15 μm length and 1-5 μm diameter. The presence of rGO/ γ-Fe_2O_3 in PANI core enhances the interfacial polarization and the effective anisotropy energy of the composite which contributes to more scattering and leads to the high shielding effectiveness (SE_T~51dB) at a critical thickness of 2.5 mm. Additionally, the effective complex permeability and permittivity parameters of composites have been evaluated from experimental scattering parameters (S_{11} & S_{21}) using theoretical calculations given in Nicholson−Ross and Weir algorithms.

1. Introduction

The recent advancement of electrical and electronic devices (TVs, computers, mobile phones, and radios etc.) has made human life easier, comfortable and luxurious. Simultaneously, the massive use of these devices generates a new kind of pollution known as electromagnetic interference (EMI). This electromagnetic (EM) pollution is not only adversely affecting the operation of electronic devices but is also being harmful to the health of human beings. Due to this, EM wave absorbing materials have attracted much attention for the proper functioning of electronics, radio frequency radiation sources in all commercial, military equipments, scientific electronic devices, communication instruments and radiation sources. Also, the EMI shielding materials should be lightweight potential absorbers of radiation field to protect aircraft avionics and health hazards in humans. Therefore, in last decades, a range of materials including very thin sheets of metals, different forms of carbon[1, 2], e.g., graphite and its exotic forms[3, 4] such as expanded graphite,[5] reduced graphene oxide (rGO)[6], carbon black[7], graphene[4], carbon fibers[8, 9], single or multiwalled carbon nanotubes (CNTs)[10], and conducting polymers, dielectric, magnetic materials and their composites have been used for EMI shielding in automotive applications. However, metals are expensive, heavy, and prone to corrosion, while adding to the complexity and cost of manufacturing processes. Therefore, as an alternative, intrinsically conducting polymer based composites with a wide range of, electrical conductivity, permittivity (ε) or permeability (μ) have been suggested for microwave absorption. Thus, EM absorption properties of various polymer composites incorporated with dielectric or magnetic materials have been widely investigated. Among the nanostructures, conducting polymers, along with some magnetic and dielectric fillers, exhibit very good EM absorption properties.

Generally, the EMI shielding effectiveness (SE) of a material depends on its dielectric properties, magnetic permeability, thickness and frequency[11]. The techno-commercial applications such as, doppler, weather radar, TV picture transmission, and telephone microwave relay systems[12] require shielding in X-band (8.2-12.4 GHz) frequency range. The EMI SE of a composite is governed by intrinsic conductivity, aspect ratio, complex permittivity and permeability of the filler[13]. The primary mechanism of shielding is the reflection loss (SE_R) which is the result of the interaction between the conducting particles in the conducting material (free electron or vacancy) and the EM field[14]. While the absorption loss depends on the value of σ_r/μ_r, i.e., the absorption loss is maximum when $\mu_r = \sigma_r$ [15, 16]. The high electrical conductivity[17], high specific surface area (surface to volume ratio)[18] of graphene make it a unique candidate to provide remarkable EMI shielding[19] in polymer composites. Due to the sp^2 bonded carbon atoms, partially rGO has good electrical response. Since graphene lacks in magnetic properties, it has only a small role in absorption of EM waves. In order to overcome this limitation, we have also synthesized nanoferrite particles on the rGO surfaces, which absorb more EM waves because of their large magnetic permeability[20-23].

Moreover, nanoferrite is not only environmental friendly but also has abundant natural supply, thus, rendering the material inexpensive.

Now a days, graphitic materials have attracted the scientific and the industrial community due to their potential applications in many areas, including EMI shielding. The graphene polymer composites is superior than the CNTs polymer composites because these are more thermally stable, hold more stiffness, lower cost (compared to CNTs), and have capability of forming a thin film, paper or coating for EMI shielding and electrostatic charge dissipation (ESD) properties. port paths. The ultra-high thermal conductivity and lower density (four times compared to copper) make graphene preferable for packing microelectronic device in the form of composite thin film, paper or coating. Our previous efforts based on graphene encourage us to search more and more new kind of composites with graphene. The present investigation is one of the most innovative efforts to discover new kind of material for EMI shielding.

To enhance the properties of conducting polymer for developing EMI shielding material, intensive efforts has been carried out on polymer ferromagnetic composites using Fe, Mn, Ni, Co ferrites and their multi-component ferrites like Fe_3O_4, Fe_2O_3, $BaFe_{12}O_{19}$, CrO_2, MnO_2, $Mn_{0.5}Zn_{0.5}Fe_2O_4$ [4, 6, 16, 24-27]. Among all of them γ-Fe_2O_3 is found to be best for developing radar absorbing materials because it offers high value of complex permeability[27, 28]. Singh et.al. have reported that super paramagnetic, nano crystalline γ-Fe_2O_3 particles and its polymer composite show Ms value of 69.0 and 20.56 emu/g at room temperature, respectively. The resulting conducting ferromagnetic composite shows microwave absorption loss of 22.8 dB [27].

The manuscript reports synthesis of γ-Fe_2O_3 decorated rGO filled in polyaniline (PANI) tube core-shell structure useful for microwave absorption. The selectivity of the different materials to synthesize present composites has been based on systematic experimental efforts as well as the associated properties of these compounds to fabricate the desired material with all required property for EMI shielding in a single composite

Previously, PANI tubes have been synthesized by several other groups because of its great potential in device applications, such as transistors,[29] sensors,[30] and batteries[31]. PANI tubes have diameter in the range of ~ 100 nm[32] and therefore, there is a possibility to fill these tubes with the materials like nanoferrite, rGO, rGO nanoferrite. PANI tubes were filled with a mixture of rGO and γ-Fe_2O_3. β-naphthalene-2-sulfonic acid (β-NSA) was used as a dopant and oxidant. The vibrating sample magnetometer (VSM) study of the composite sheets with different amounts of γ-Fe_2O_3 enabled us to understand their magnetic induction behavior and hence, its effect on EMI shielding. The composite pellets having thickness critical 2.5 mm have shown high value of SE ranging from 21.49 to 53.83dB (~99.99%) in the microwave range (X-band). Such novel composite may find potential applications such as EMI shielding, ESD, gas sensor etc.

2. Experimental

2.1 Materials

Aniline, ammonium persulfate (APS), hydrazine hydrate by Rankem Limited, India, Ferric acetylacetonate ($Fe(acac)_3$), methanol, H_2SO_4 by Merck, India, β−NSA by Himedia, HNO_3 by Fisher Scientific and natural graphite powder (purity 99.5%, particle size 50 μm) were procured from Loba Chemie, India. The aniline monomer was purified by distillation under reduced pressure before use. Aqueous solutions were prepared using double deionized water having specific resistivity of 10^6 Ω-cm. The other chemicals were of reagent grade and used as received.

2.2 Synthesis of rGO/γ-Fe_2O_3 incorporated polyaniline (PRF) composite

The chemical oxidative polymerization of aniline was carried out in the presence of γ-Fe_2O_3 decorated rGO (RF) particles to prepare PRF composites. Prior to PRF synthesis, In-situ synthesis of γ-Fe_2O_3 nanoparticles on the rGO matrix were carried out by taking 1:1 wt. ratio of rGO and $Fe(acac)_3$ and the resultant composite were abbreviated as RF. The synthesis of RF and rGO were discussed in detail in our earlier report.[6] β−NSA was used as a dopant without an external template. This method belongs to the self-assembly process[12] because β−NSA works as a dopant and a template functioning at the same time. A typical preparation process for PANI-RF composite is as follows: 0.3 M solution of β−NSA and calculated amount of RF was homogenized (ART MICCRA D8 rotating at 17600 rpm for 2-h,) to obtain a uniform suspension containing RF particles. 0.1 M aniline has been added and stirring continued for another 1h to form an emulsion. The aniline-β-NSA mixture containing RF particles were cooled in an ice bath for 2-h before oxidative polymerization. Finally, the oxidant APS (0.1 M) was added drop wise to the above solution keeping the temperature of the reactor at 0°C with vigorous stirring for 10-h. The green polymer precipitates so obtained were treated with methanol in order to remove oligomers. The resulting precipitate was filtered and washed thoroughly till the filtrate became colorless and then dried at 60−65°C in a vacuum oven for 24-h. Throughout the experiment, the molar ratio of aniline to β-NSA and APS was retained at 1:3 and 1.0, respectively. However, the concentration of RF particles was changed to understand the effect of RF particles on the morphology, structure, electrical properties and shielding effectiveness of the resulting PANI-PRF composite tubes. Such a cooperative combination of β-NSA (a non-corrosive organic dopant having surfactant traits), RF nanoparticles (conducting, magnetic and dielectric filler or guest) and PANI (electrically conducting matrix or host), can offer advantages such as good electrical, magnetic and dielectric properties which may collectively contribute towards high microwave absorption efficiency. Several compositions having different AN:RF weight ratios, i.e., 1:0, 1:1, 1:2 and 1:3, were prepared and designated as PRF10, PRF11, PRF12 and PRF13, respectively.

2.3 Materials Characterization

The morphology of PANI-β-NSA tubes and its composites were examined using scanning electron microscope (SEM, Zeiss EVO MA-10). The SEM samples were prepared by dispersing the powder in iso-propanol using ultra-sonication and placing small drops of the suspension on silicon wafers and sputter-coated with gold before analysis. High-resolution transmission electron microscope (HRTEM) was taken using Technai G20-stain 300kV instrument. The semi crystalline nature of PANI-β-NSA and PRF composite was confirmed by X-ray diffraction (XRD) studies[13] carried out on D8 Advance XRD (Bruker) using CuKα radiation (λ= 1.54Å) in the scattering range (2θ) of 10°-70° with a scan rate of 0.02°/sec and slit width of 0.1mm. the electrical conductivity of PRF composites were examined by a well established four-probe method using computer controlled Keithley current source (Model 6221) and nanovoltmeter (Model 2182A) at room temperature. For electrical conductivity measurements, rectangular pellets ($13\times7mm^2$) were prepared from powder sample using rectangular die and hydraulic press at compression pressure of 5 ton. Four ohmic contacts were made on the corners of pellet using silver epoxy paste. The thermal stability of the composite was performed by Thermogravimetric analyzer (Mettler Toledo TGA/SDTA 851°)[13] under inert atmosphere (flowing N_2 gas) in the temperature range 25-900°C. FTIR spectra were recorded on Nicolet 5700 in transmission mode in the wave number range 400-2000 cm^{-1}. The spectroscopic grade KBr pellets were used for collecting the spectra with a resolution of 4 cm^{-1} performing 32 scans. Raman analysis was carried out using Renishaw in Via Reflex spectrometer, UK with an excitation source of 514.5 nm. The resolution of the instrument was less than 1.0 cm^{-1}. To explore the EMI shielding dielectric measurements of the composite Agilent E8362B Vector Network Analyzer was used in the X-band. The Powder samples were pelletized in rectangular shape with dimension 22.8*10 mm^2 of thickness ~2mm and inserted into copper sample holder connected between the wave-guide flanges of network analyzer.

3. Results and discussion

The RF filled PANI nanocomposites (PRFs) have been prepared by in-situ emulsion polymerization using β-NSA as anionic surfactant molecule which also acts as a dopant. Due to its amphiphilic and surfactant nature, β-NSA molecule (with hydrophilic SO_3H head and hydrophobic tail) easily forms micelles in aqueous solution. As discussed in the experimental section, RF particles were dispersed in β-NSA aqueous solution before polymerization. As a result, micelles containing RF particles form in the reaction, these micelles have core-shell structure. 0.1 M aniline monomer was added to above emulsion and homogenized for another 1-h. During this, aniline reacts with β-NSA to form aniline/β-NSA micelles which act as a soft template with the formation of oil in water type emulsion. Afterward the homogenized mixture was transferred to double walled glass reactor, pre-cooled to -5ºC. Polymerization was initiated by dropwise addition of water soluble oxidant, i.e., APS and allowed to continue at -5°C under continuous stirring. During this process the formed anilinium cations might be absorbed on the plane of these core-shell micelles. Furthermore, free aniline present in the solution might diffuse into the micelles to form aniline-filled micelles. Therefore, these micelles (with or without RF) act as soft templates for the formation of the tube like structure. The attached -SO_3H groups impart additional dopant property to β-NSA. As the polymerization advances, the micelles containing RF particles would become bigger spheres and take the shape of tubes/rods by elongation. Therefore, subsequent oxidation of aniline results radical cations which combine with another unit to form neutral dimer. Further oxidation of Dimer leads to the formation of a trimer, tetramer and finally the formation of polymer composites. Scheme 1 discussed self-assembly process resulting in tube like structure of PANI and PRFs composite [33, 34] and suggests that RF particles should be situated inside the polymer tubes. Schematic representation of incorporation of RF into PANI matrix is given in this scheme which suggests that rGO and γ-Fe_2O_3 embedded in PANI tubes leads to the formation of PANI composites which has better electrical and magnetic properties. The presence of rGO containing iron oxide nano particles in polymer matrix has been confirmed by the XRD of the composites. The presence of γ-Fe_2O_3 magnetic nanoparticles in RGO matrix has been confirmed by TEM.

3.1. SEM analysis

SEM has been carried out to determine the distribution of rGO or rGO platlets and γ-Fe_2O_3 in the polymer matrix. Figure 1 (a) shows the agglomerated magnetic nanoparticles derived from thermal decomposition of $Fe(acac)_3$. The estimated particle size of rGO has been found up to few micrometer as shown in Figure 1 (b). Although, thickness of rGO sheets and particle size of γ-Fe_2O_3 have not been possible to explore via SEM technique. The inset show the distribution of nanoparticles of γ-Fe_2O_3 on the surface of rGO sheet. SEM image of PANI composites synthesized in the presence of β–NSA reveal an interesting morphology featuring formation of tube like structure (Figure1(c)). Densely packed tubes have a range of diameter and length of ~0.5 to 2μm and up to 15μm, respectively. SEM micrograph of PANI composites reveals that RF particles are entrapped within the PANI matrix (Figure 1 (d)). This reduces the length of the tubes and increases the roughness of the surface. The diameter of PANI composite is larger than the pristine PANI.

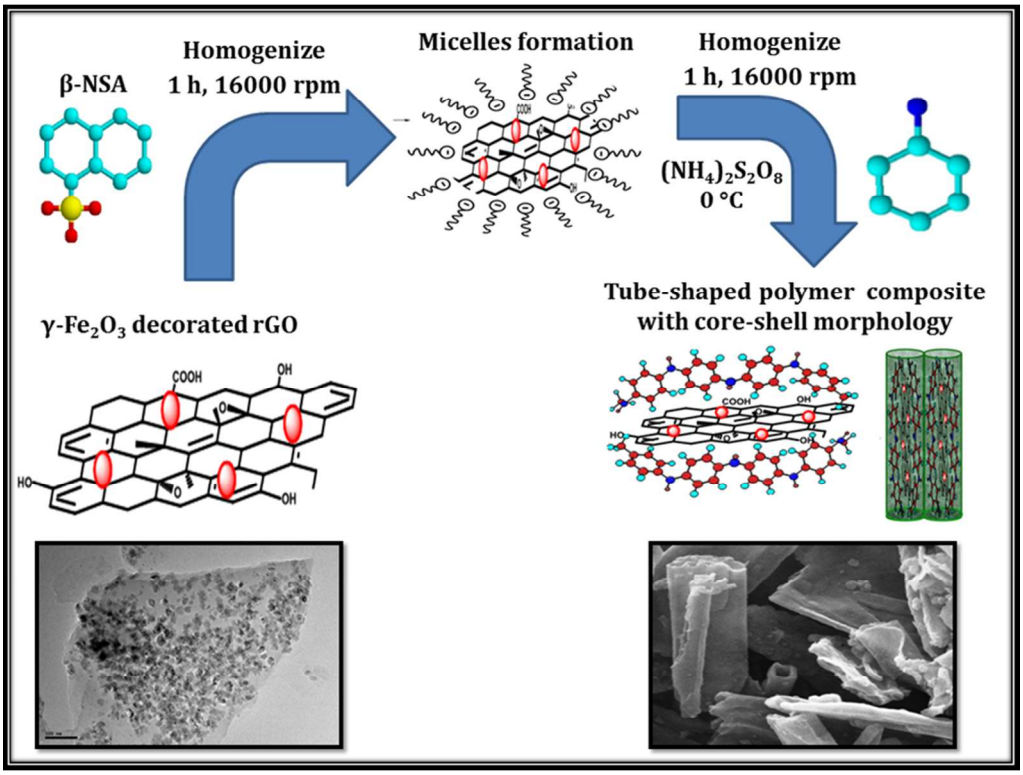

Scheme 1 Schematic representation of fabrication of γ-Fe_2O_3 nanoparticles decorated rGO sheets filled in PANI tubes by *in-situ* polymerization of aniline using APS as oxidant in the presence of β-NSA

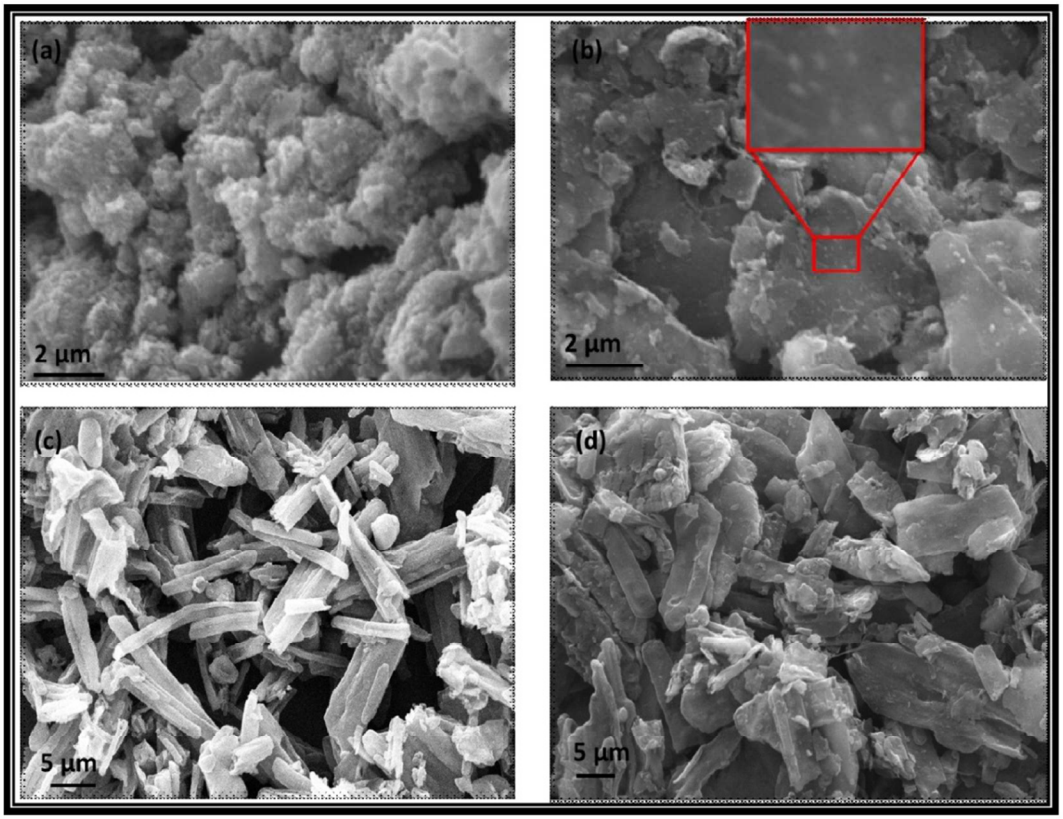

Figure 1 SEM images of (a) iron oxide nanoparticles derived from $Fe(acac)_3$ by thermal decomposition at 186 ºC, (b) reduced graphene oxide sheets decorated with γ-Fe_2O_3 nanoparticles, (c) PRF10 and (d) PRF13, showing the formation of tube like structure with RF particles inside the tubes

3.2 TEM analysis

Figure 2 demonstrates the TEM/HRTEM images of γ-Fe_2O_3, rGO sheet, RF, pristine PANI and PANI composites. Figure 2 (a) shows the iron oxide nanoparticles derived from $Fe(acac)_3$ by thermal decomposition at 186 ºC in an organic solvent. The lattice plane spacing of the γ- Fe_2O_3 particles is about 0.29 nm which corresponds to the 206 plane as shown in Figure 2(b). It was first confirmed with the XRD pattern of the γ-Fe_2O_3 phase. Figure 2(c) shows the HRTEM image of a few rippled rGO nanosheets which clearly indicates the graphitic lattice. The interplanar distance has been measured to be 0.37 nm, corresponding to the spacing of the 002 planes. This is consistent with the result calculated from XRD analysis, Figure 3 (a). The dispersion of γ- Fe_2O_3 in rGO matrix is confirmed by the HRTEM image (Figure 2 (d)). Figure 2 (e) shows the PANI tubes having diameter ~1.75 µm and length ~6 µm. PANI tubes are filled with a mixture of nanoferrite particles and rGO. Diameter of PANI composite is more in comparison of the pristine PANI tubes (Figure 2 (f)). The presence of rGO (conducting filler) and γ-Fe_2O_3 nanoparticles (magnetic filler) in the core of PANI is helpful for improving matching of ε_r and μ_r which is necessary for enhancing the absorption of the EM wave.

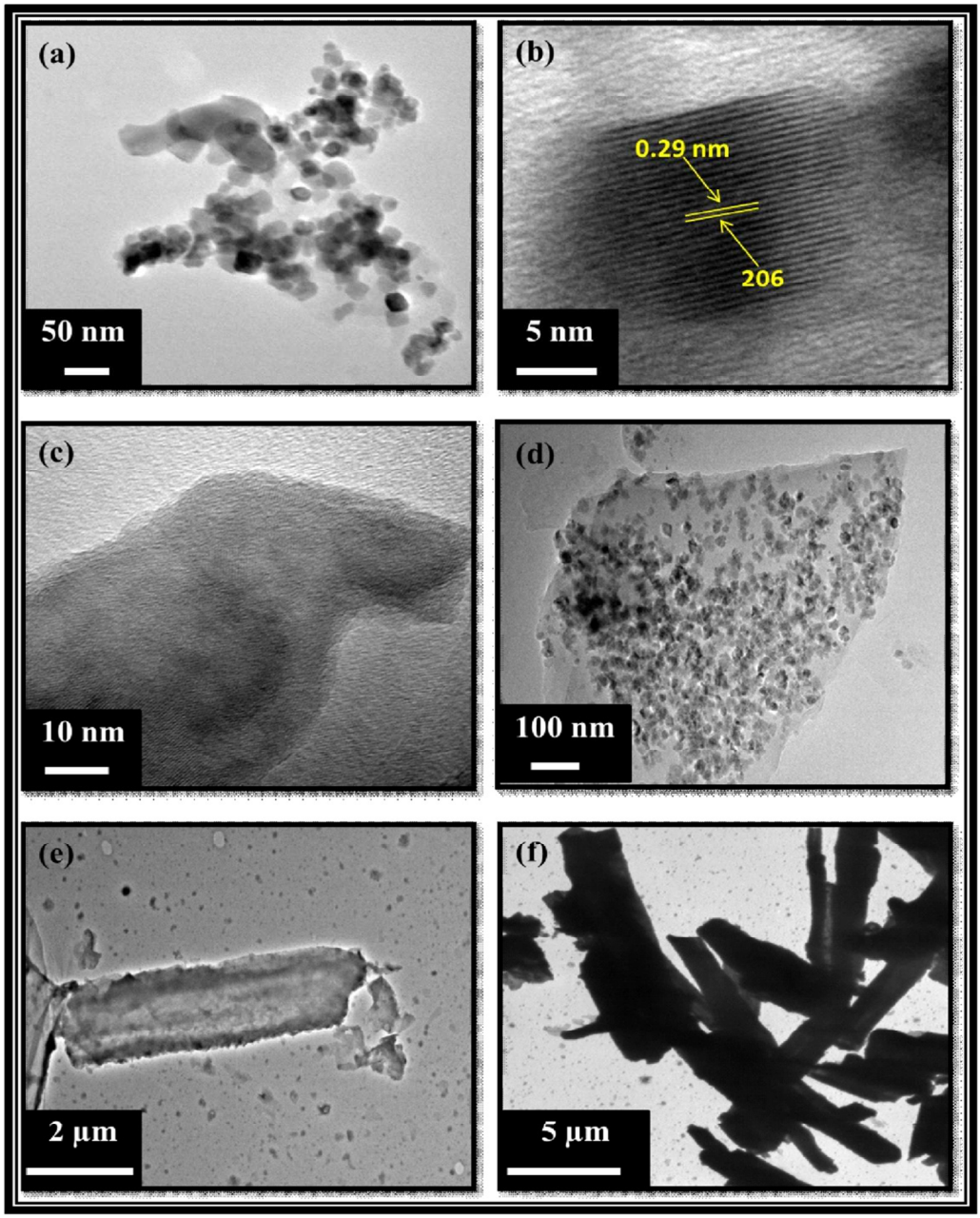

Figure 2 (a) TEM image of γ-Fe_2O_3, (b) High magnification HRTEM image of γ-Fe_2O_3 showing the 206 oriented lattice planes of γ-Fe_2O_3, (c) TEM image of rGO sheets, (d) TEM image of rGO-γ-Fe_2O_3 hybrid structure, showing the nanoparticles of γ-Fe_2O_3 on the rGO surface, (e) TEM micrographs of pristine PANI tube and (f) PANI tubes filled with a mixture of rGO-γ-Fe_2O_3

3.3 XRD Analysis

Figure 3 (a) shows the XRD patterns of γ- Fe_2O_3, RF, pristine PANI, and PANI composite. The main peaks for γ-Fe_2O_3 are observed at 2θ=30.265° (d=2.9530 Å), 2θ=35.659° (d=2.5177 Å), 2θ= 43.320° (d=2.0886 Å), 2θ=57.321° (d=1.6073 Å) and 2θ=62.981° (d=1.4758 Å) corresponding to the (2 2 0), (3 1 1), (4 0 0), (5 1 1) and (4 4 0) reflections, respectively. All observed peaks of γ-Fe_2O_3 have been matched with the standard XRD pattern (Powder Diffraction File, JCPDS No. 39–1346). The peaks present in γ-Fe_2O_3 have also been observed in iron incorporated rGO composite sheets which indicate the presence of ferrite particles in the rGO matrix. The presence of rGO is confirmed by the broad peaks at 2θ=26.441° (d=3.368), 2θ=54.599° (d=1.679 Å). PANI shows two broad peaks at 2θ=19.795° (d= 4.481 Å) and 25.154° (d = 3.537Å), which reveals its amorphous nature.[33] The peaks of RF observed in PRF13 confirm the presence of a RF hybrid in the polymer matrix. The crystallite size of γ-Fe_2O_3 particle can be calculated by using Debye Scherrer's formula, D=kλ/βCosθ, where, D is crystalline size, λ is the X-ray wavelength, K the shape factor, θ is the half angle in degrees, and β is the line broadening measured by half-height in radians. The value of k is often assigned a value of 0.89, which depends on several factors, including the Miller index of the reflecting plane and the shape of the crystal. The average size of γ-Fe_2O_3 particles has been calculated using the above equation and estimated as 8.99 nm for pure γ-Fe_2O_3 and 9.83 nm for iron incorporated rGO. The peaks at 2θ=30.265° (d=2.9530 Å), 2θ=35.659° (d=2.5177 Å) for γ-Fe_2O_3 in the PANI composites show the formation of composites having separate phases of both compounds properly dispersed in the polymer matrix.

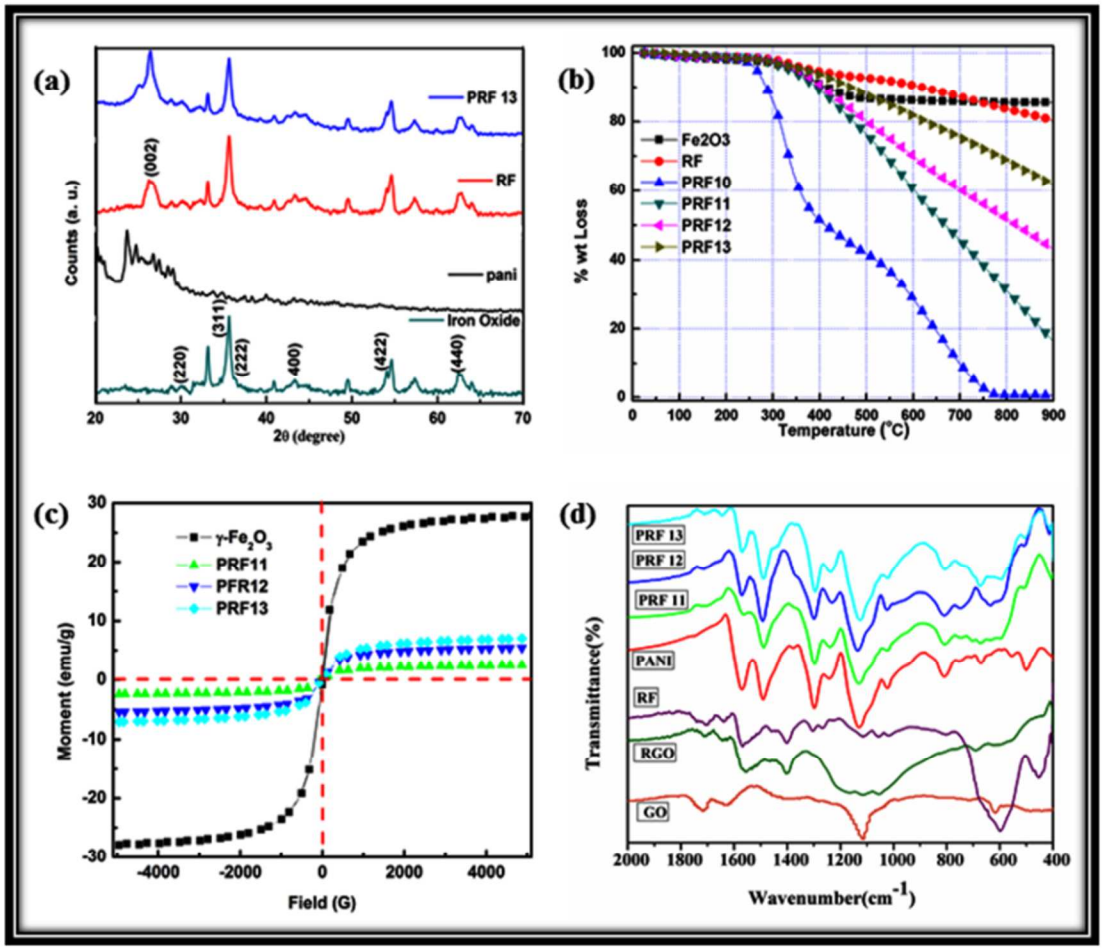

Figure 3. (a) XRD of γ-Fe_2O_3, pristine PANI, RF and PRF13, (b) Thermogravimetric (TG) plots of PANI–RF composites with different RF contents in N_2 atmosphere, (c) Vibrating sample magnetometer plots of γ-Fe_2O_3 and PANI composites (d) comparison of FTIR spectra of GO, rGO, RF, PRF10, PRF11, PRF12, and PRF13

3.4 TGA Analysis

TGA of the PANI doped with β–NSA and PANI composites has been carried out in order to see the effect of the RF content on the thermal stability of the composite (Figure 3 (b)). Pure RF is thermally stable up to 303 ºC and weight loss has been only 2%. The PANI composites show multistep weight loss corresponding to loss of different species. The first loss step at 120 ºC is due to the loss of water and other volatiles. The second loss in the range of 230–380 °C is due to the loss of the $–SO_3H$ functional group of dopant and the onset of polymer

degradation. The final major loss step (380° to 700 °C) has been attributed to the complete degradation of dopant as well as the polymeric backbone. Initial decomposition temperature (IDT) where degradation reactions first started, has also been affected by increasing RF content. The PANI doped with β−NSA (PRF10) has been found to be thermally stable up to 237°C. However, when conducting polymer has been synthesized by incorporating RF in (PRF11), it has been observed that the thermal stability of the polymer increases to 273°C. This shows that, in-situ polymerization of aniline in the presence of RF particles leads to a more thermally stable conducting polymer. The approximate amount of incorporated RF in composites has been calculated by subtracting the wt.% char residue (at 900 °C) of the blank polymer from that of the respective composites. It has been observed that in the three different compositions, PF10; PF11; PF12 and PF13; the wt.% of RF has been estimated to be 0, 20.17, 43.15 and 60.55% which is in accordance with the amount taken during synthesis.

3.5 Magnetic properties

The field dependence of magnetization for the PANI composite containing different wt.% of rGO decorated with γ-Fe_2O_3 nanoparticles have been studied by using the M–H curve at room temperature as shown in Figure 3(c). The saturation magnetization (Ms) value of the γ-Fe_2O_3 has been found to be 29.15 $emug^{-1}$ at an external field of 5 kOe having a small value of coercivity and negligible retentivity with no hysteresis loop, indicating a super paramagnetic nature. When these nanoferrite particles are incorporated in the rGO matrix in 1:1 weight ratio, the Ms value has been found to be 16.25 $emug^{-1}$. Furthermore, it is expected that Ms value may greatly decrease of PANI composites (e.g. in PRF11 Ms value decreases from 16.25 to 2.47 $emug^{-1}$) because iron oxide is encapsulated in polymer tubes. The role of the tube thickness is important to control the sufficient magnetization value which is required for EMI shielding applications. We have done several trial to optimize the concentration of polymer in the composite to control the magnetization, efficient capping as well as optimum conductivity for shielding application Ms values of different PANI composites have been measured and given in the Table 1 (see supporting material document). The ferromagnetic properties of composites further confirm that the oxide in the present investigation is γ-Fe_2O_3 rather than Fe_3O_4 which is also supported by the XRD pattern. Ms value of PANI composite increases with the increase of RF loading due to the higher content γ-Fe_2O_3.

3.6 FTIR Spectroscopy

Figure 3 (d) demonstrates the FTIR spectra of GO, rGO, RF, PRF10, PRF11, PRF12, and PRF13. The spectrum of GO shows the presence of various oxygen-containing functional groups; characteristic peaks at 1725 and 1105 cm^{-1} have been assigned to C=O from carboxyl (COOH) and (C-O-C) groups from epoxide, respectively. The peak at 1630 cm^{-1} arises due to the contributions from the skeletal vibrations of unoxidized graphitic domains or the remaining sp^2 carbon character of graphite (C-C). However, in the case of RGO, RF and PANI composites, most of the oxygen-containing functional groups decrease or disappear which confirms the efficient reduction of GO. In the FTIR spectra of PANI (PRF10), bands near 1460 and 1570 cm^{-1} are assigned to the C=C stretching of the benzenoid and quinoid rings, respectively. The peak at 1300 cm^{-1} is assigned to the C-N stretching of the secondary amine, a characteristic band of the conducting emeraldine salt form of PANI originating from a bipolaron structure related to the C-N stretching vibration. The band at 1130 cm^{-1} can be assigned to an in plane bending vibration of the C-H (mode of N=Q=N, Q=N^+H-B, and B-N^+H=B), which is formed during protonation. Hence, these FTIR spectra correspond to a well-doped emeraldine salt. The band at 670 cm^{-1} (Fe-O stretching) confirms the formation of γ-Fe_2O_3 on the graphene sheets.

3.7 Raman Spectroscopy

Raman spectroscopy is an important tool to identify the proper interaction or bonding between two components[35]. Figure 4 shows the Raman spectra of RGO, RF, PRF10, and PRF13. The Raman spectra of RGO consist of three prominent characteristic peaks, namely the D band, the G band, and the G' (2D) band confirming the formation of RGO. Inset of the Figure 4 shows the Raman spectrum of pure γ-Fe_2O_3 which reveals all the characteristic bands of γ-Fe_2O_3 in the low frequency region, i.e., Eg mode (245, 294, 301, 422, 611), A1g mode (513) confirming the presence of γ-Fe_2O_3.[36] A broad 2D peak due to the presence of RGO has been observed in all three spectra of RGO, RF and RF13 and a slight right shift in the peak position from RGO and RF to RF13 has also been observed. The bands at 1167 and 1623 cm^{-1}, assigned to C–H, and C–C of benzenoid units, respectively, have been observed in PANI spectrum (PRF10)[37]. The same bands have been observed for PANI composites with a slight blue shift, i.e., 1167 to 1172 cm^{-1} and 1623 to 1625 cm^{-1}. Another band at 1321 cm^{-1} related to C–N stretching modes of delocalized polaronic charge carriers which is characteristic of the protonated imine form of PANI[38,] has

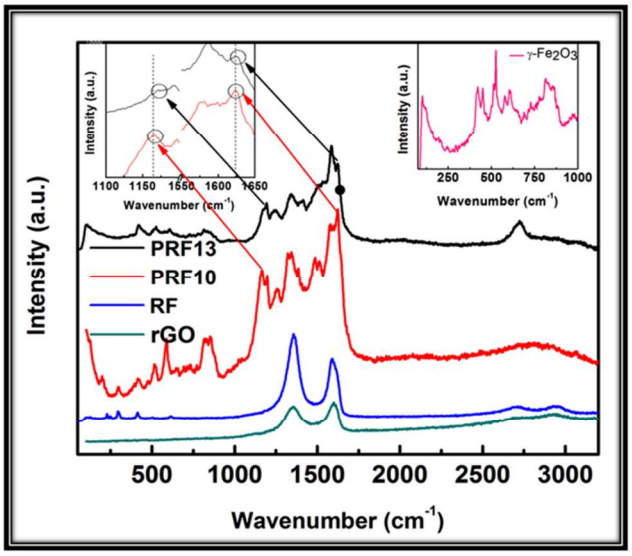

Figure 4. Raman spectra of rGO, RF, PRF10, PRF13 and Inset image shows the raman spectra of γ-Fe_2O_3

also been observed. This band has shifted to 1342 from 1321 cm^{-1} with the incorporation of RF. Slight shifting in the bands is an evidence of interaction between these components. In addition to this, the low frequency mode of γ-Fe_2O_3 hss also been seen in RF and PRF13 samples due to the presence of γ-Fe_2O_3 in the material..

3.8 Conductivity

The room temperature electrical conductivity of composites (Table 1) increases sharply on higher loading of γ-Fe_2O_3 decorated rGO, i.e., from 21.49 Scm^{-1} (PRF10) to 53.83 Scm^{-1} (PRF13). This is attributed to two reasons. Firstly, the rGO sheets possess very good conductivity. Secondly, the conducting network is improved on higher wt% loading of RF particles resulting in enhancement of electrical conductivity of the composites. Most importantly, these samples show optimum value of conductivity and magnetization which is desired for exhibiting good microwave shielding responses.[6, 39]

3.9 Electromagnetic shielding & dielectric studies.

The EM parameters, i.e., relative complex permittivity (ε*=ε′-iε″) and relative complex permeability (μ*=μ′-iμ″) have been measured at room temperature for the study of microwave absorption properties of PANI composites which are shown in Figure 5 (a-f). These obtained complex parameters have been estimated from experimental scattering parameters (S_{11} & S_{21}) by standard Nicholson-Ross and Weir theoretical calculations [40].

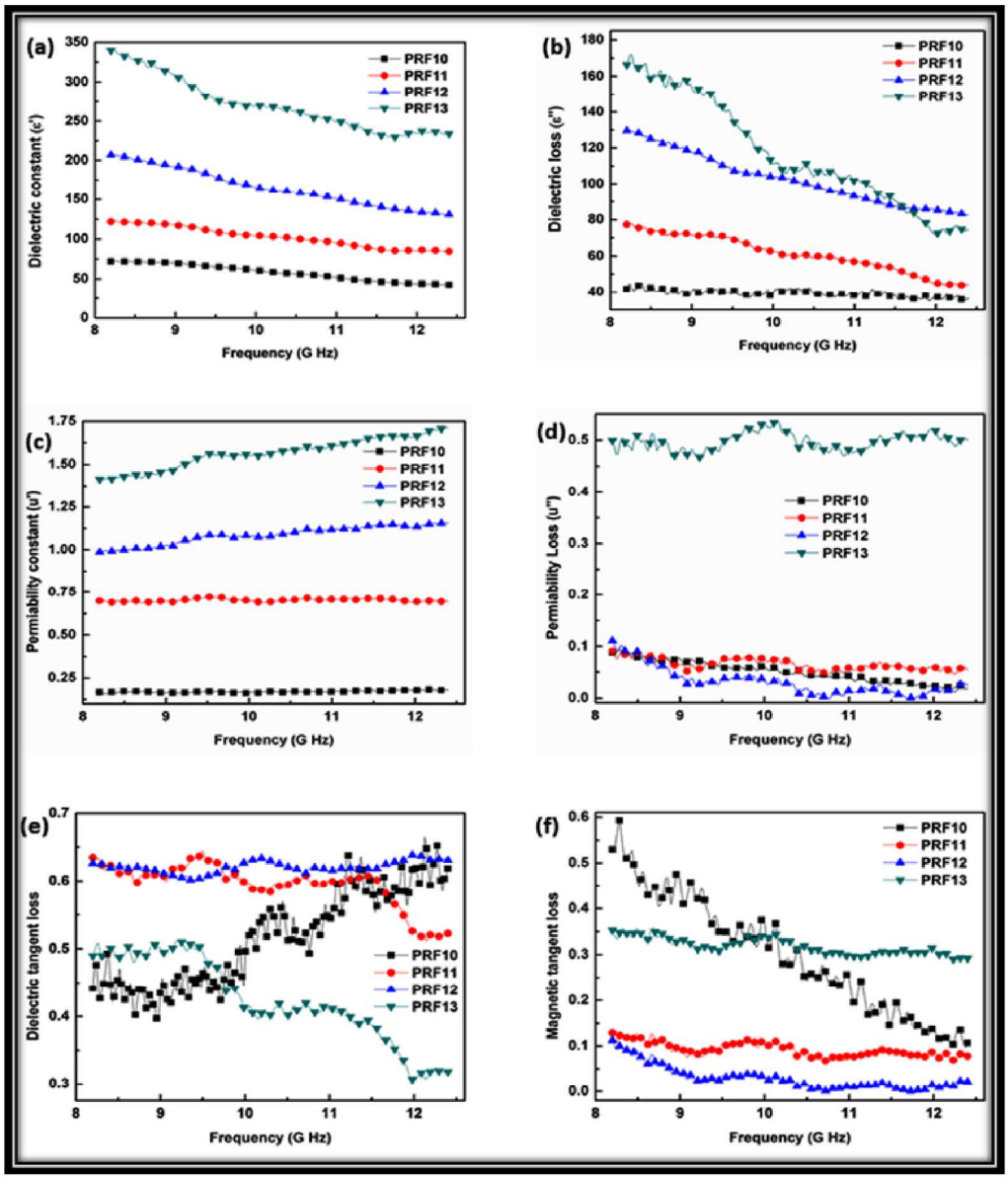

Figure 5. Frequency dependence of the (a) real parts and (b) imaginary parts of the complex permittivity, (c) real parts and (d) imaginary parts of permeability and the corresponding (e) dielectric loss tangents and (f) magnetic loss tangents of PANI composites

The estimated real part of the EM parameters (ε′, μ′) is directly associated with the amount of polarization occurring in the material which symbolizes the storage ability of the electric and magnetic energy, while the imaginary part (ε″, μ″) is signifies the dissipated electric and magnetic energy.

From Figure 5 (a), for PANI composites PRF11, PRF12 and PRF13, the values of ε′ are in the range of 121.82-84.68, 206.94-130.93, and 339.45-233.77, respectively, which are higher than the pristine PANI (71.94-42.60) in the frequency range 8.2 to 12.4 GHz. Meanwhile, the value of ε″ for PRF11, PRF12 and PRF13, are in the range of 77.35-44.27, 129.60-82.58 and 166.28-74.39, respectively, which are also higher than pure PANI (41.78-36.35) as shown in Figure 5 (b). It is observed that the samples with higher wt% loading of RF show higher values of ε′ and ε″ due to higher conductivity of RF. It is proposed that more rGO plates may enhance the conductivity and electric polarization because the relative complex permittivity is a measure of the polarizability of a material which induces dipolar and electric polarization in the presence of microwave.

As shown in Figure 5 (c) for PANI composites PRF11, PRF12 and PRF13, the values of μ′ are in the range of 0.69-0.70, 0.98 1.15 and 1.41-1.71, respectively, which are higher than the pristine PANI (0.16-0.18,) in the X-band. Meanwhile, the value of μ″ for PRF11, PRF12 and PRF13 are in the range of 0.09-0.05, 0.11-0.02 and 0.49-0.50 respectively, which are almost equal to pure PANI (0.08-0.02), as shown in Figure 5 (d). Dielectric tangent loss (tan δ_E = ε″/ε′) and the magnetic tangent loss (tan δ_M= μ″/μ′) of PANI composites are also calculated using the permittivity and permeability parameters of the samples and presented in Figure 5 (e) and (f), respectively. The observed tan δ_E is always greater than 0.3 in the entire frequency range indicating that the dielectric loss occurs in all frequency ranges. These results suggest that PANI composites have distinct dielectric loss properties.

According to, the EM theory, dielectric losses are the result of complex phenomena like natural resonance, dipole relaxation, electronic polarization and its relaxation, polarization of polarons and bipolarons in the polymer matrix and their relaxation and certainly the unique structure of the shield. Iron oxide nanoparticles decorated rGO sheet, due to its high conductivity, act as a polarized centre inside the PANI tube which results in more microwave absorption. High aspect ratio of the PANI tubes filled with RF nanoparticles having high conductivity also enhances the absorption properties. In PANI composites, the existence of interfaces between iron oxide nanoparticles and rGO layer, iron oxide and PANI as well as between rGO and PANI. Ferromagnetic nanoparticles act as tiny dipoles which get polarized in the presence of EM field and result in better microwave absorption.

PANI and RF nanoparticles and between PANI-PANI tubes, are responsible for interfacial polarization which further contribute to dielectric losses. Interfacial polarization occurs in heterogeneous media due to accumulation of charges at the interfaces and the formation of large dipoles. Figure 5 (b) shows that ε″ increases with the higher wt.% loading of RF, this is attributed to a conducting network formed by nano ferrite particles decorated rGO sheets. In addition, the conductivity of the samples is further improved by conducting PANI tubes and results in the increase of dielectric loss. Moreover, the dielectric loss is also improved by polaron and bipolaron hopping in PANI matrix which has been reported earlier.[41] The magnetic loss (tan δ_M) is a result of eddy current effects, natural resonances and anisotropy energy present in the composites. In the microwave ranges, the presence of nano ferrite particles in the composite are the main cause of eddy current. The natural resonances in the X-band can be attributed to the small size of γ-Fe_2O_3 on the rGo sheet. Anisotropy energy of the small size materials,[42] especially in the nanoscale, would be higher due to surface anisotropic field due to the small size effect.[43] The higher anisotropy energy also contributes in the enhancement of the microwave absorption.

EMI SE of any material can be expressed as[4, 6, 25, 27, 41, 44]

$$SE(dB) = \mathrm{SE_R} + \mathrm{SE_A} + \mathrm{SE_M} = 10\log(P_T / P_I) = 20\log(E_T / E_I) \quad (1)$$

where, P_I (E_I) and P_T (E_T) are the power (electric field intensity) of incident and transmitted EM waves, respectively. The terms in equation 1 can be defined as

$$SE_R = -10\log(1-R) \quad (2)$$

$$SE_A = -10\log(1-A_{eff}) = -10\log(T/1-R) \quad (3)$$

SE_R, SE_A and SE_M represents shielding effectiveness due to reflection, absorption and multiple reflections respectively, The correction term SE_M can be ignored in all practical application when SE >10 dB [45, 46].

Therefore, the effective absorbance (A_{eff}) can be described as $A_{eff} = (1-R-T)/(1-R)$ with respect to the power of the effectively incident EM wave inside the shielding material.

For a material, the skin depth (δ) is the distance up to which the intensity of the EM wave decreases to 1/e of its original strength. The δ is related to angular frequency, relative permeability and total conductivity $\sigma_T = (\sigma_{dc} + \sigma_{ac})$. According to EM theory, for electrically thick samples (t>δ), frequency (ω) dependence of far field losses can be expressed in the terms of total conductivity (σ_T), real permeability (μ'), skin depth (δ) and thickness (t) of the shield material as: [46]

$$SE_R(dB) = 10\log\{\sigma_{ac} / 16\omega\varepsilon_0\mu'\} \quad (4)$$

$$SE_A(dB) = 20\{t/\delta\}\log e = 20d\sqrt{\mu\omega\sigma_{ac}/2}\log e = 8.68\{t/\delta\} \quad (5)$$

The σ_{ac} and δ can be related to the imaginary permittivity (ε") and real permeability (μ') as $\sigma_{ac} = \omega\varepsilon_o\varepsilon''$ and $\delta = \sqrt{2/\sigma\omega\mu'}$ which gives absorption loss as:

$$SE_A(dB) = 8.68t\sqrt{\sigma\omega\mu'/2} \quad (6)$$

SE_A becomes more dominant as compared to the SE_R in the microwave range. This may be caused by the shallow skin depth and high conductivity (σ_{ac}) values at such high frequencies[45, 46] Figure 6 (a) shows the variation of the SE with frequency in the 8.2-12.4 GHz range. From the experimental measurement, the SE due to absorption (SE_A) of PANI composites has been found to vary from 17 to 43 dB with increase in the γ-Fe_2O_3 content while the SE_R remains nearly constant at 9 dB. Thus, the total SE achieved for the composite is 51 dB (PRF13) which is higher than the pristine PANI (PRF10). It has been observed that for conducting PANI composite, SE is mainly dominated by absorption while the

SE_R is constant. It is observed that the thickness of the shield has a great influence on the microwave absorbing properties as shown in Figure 6 (b). Our PANI composites exhibit better microwave absorption properties in comparison with pristine PANI,[33] pure rGO, γ-Fe_2O_3 nanoparticles,[47] PANI-γ-Fe_2O_3 composite,[47] PANI/multiwall carbon nanotubes composite,[48, 49] PANI rGO iron oxide composites[50] reported earlier.

To relate σ_{ac} with the shielding parameter of the material, SE_A has been plotted against $(\sigma_{ac})^{1/2}$, (Figure 6 (c)). The skin depth of the samples has been calculated using the relation, $\delta = \sqrt{2/\omega\mu\sigma_{ac}}$ and its variation with frequency has been shown in Figure 6 (f). It can be noticed that the skin depth is constant in the overall frequency range which demonstrates the surface conduction as shown in figure exists in the whole frequency range. The Skin depth of PANI composite is very small (600 μm), due to the high electrical

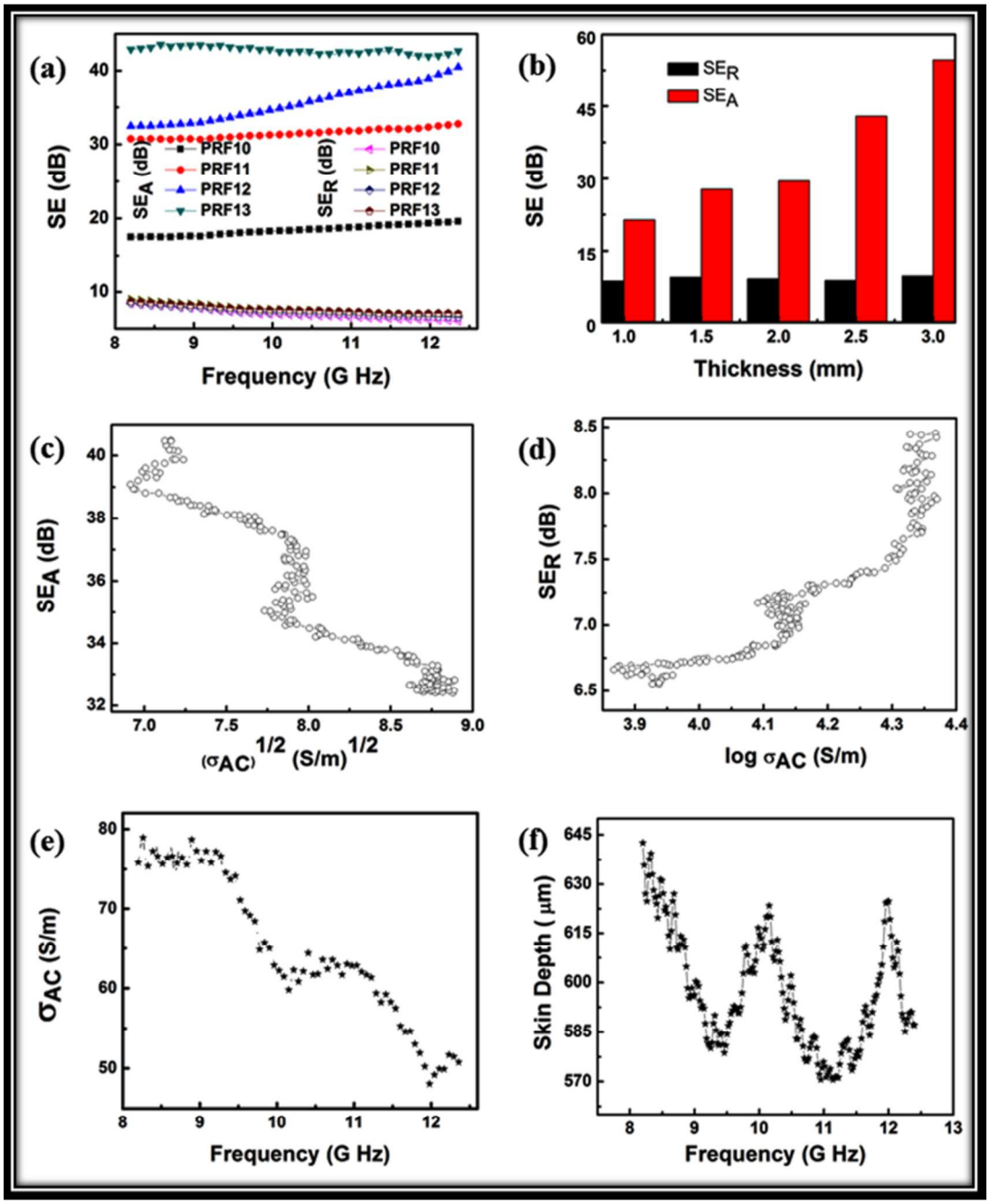

Figure 6. (a) EMI SE of PANI composites having different wt.% ratio of RF, (b) SE of PRF13 composite with different thickness, (c) dependence of SE_A as a function of $(\sigma_{ac})^{1/2}$ while (d) variation of SE_R as a function of log σ_{ac}, (e) shows the variation of σ_{ac} with the increase in frequency and (f) shows change in skin depth with increase in frequency for the sample PRF13

conductivity and good magnetic properties. From equation 6, it is seen that better SE_A can be achieved from moderate conducting materials. The dependence of SE_R as a function of log σ_{ac} is shown in Figure 6 (d) while Figure 6 (e) shows the variation of σ_{ac} with the increase in frequency for the sample PRF13 calculated from the dielectric measurements ($\sigma_{ac}=\omega\varepsilon_0\varepsilon''$). Therefore, moderate value of conductivity (σ_{ac}) is required for materials having less SE due to reflection.

Reflection loss have also been calculated from experimental S parameter (S_{11}) using "Agilent E83628 PNA Vector Network Analyser". Measurements have been performed according to Belaabed et. al.[16] The wave guide is fitted with the sample backed by a metal short (see supporting material document). The wave absorption property can be deduced from the measurement of the reflection loss RL (S_{11}) given by the network analyzer:

$RL = 20 \log (S_{11})$

The minimal reflection of microwave energy can be attributed to the dip in RL. It was observed that the composites indicate a value of ~ 2.5 to 3.25 (-dB) reflection loss at 10 GHz frequency. These results demonstrate that the intensity and the frequency of the microwave energy absorption for the composite also depend on the rGO and iron oxide content in the PANI. Thus, microwave absorption properties of composite are improved by the dielectric and magnetic losses. The reflection loss of PANI-rGO/iron oxide hybrid composites as a function of frequency at different filler's amount is given in supporting material document.

The excellent microwave absorbing performance of PANI composites is mainly attributed to two factors: impedance matching and EM wave attenuation. The ideal condition for the perfect absorber is $\varepsilon_r=\mu_r$, the presence of rGO sheet decorated with insulating magnetic γ-Fe_2O_3 nanoparticles in the core of PANI matrix has lowered ε_r of the composite, and improved the equality of ε_r and μ_r, which helps the level of impedance matching.[16] Also, PANI composites have strong microwave absorption due to their dielectric and magnetic loss. Furthermore high aspect ratio of PANI tubes, the existence of residual defects in γ-Fe_2O_3 nanoparticles decorated rGO sheet[51] and multiple reflections with in the shield enhances the microwave absorption ability of the composites. To further give a visual demonstration of the microwave absorption mechanism as discussed above a schematic is given in Scheme 2. From all the above, the results of PANI composites illustrates that these composites could be used as microwave absorbing material.

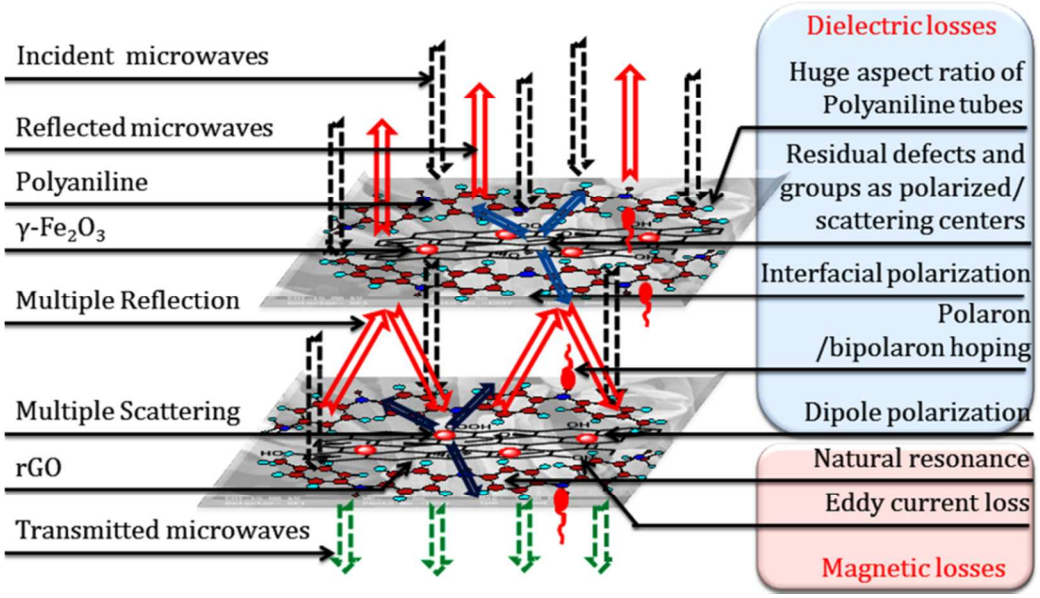

Scheme 2. Schematic presentation of possible microwave absorbing mechanisms in the PANI composites

4. Conclusion

PANI micro tubes filled with a mixture of rGO/γ-Fe_2O_3 have been successfully synthesized using micro emulsion method which results in a core–shell tubular structure. The detailed micro-structural/structural characterizations as well as the characteristics of this core-shell tubes has been examined by SEM, TEM, XRD, FTIR, Raman, UV, TGA and VSM. The core-shell tubular structure associated with RF particles embedded in polymer chains attributes the enhanced interfacial polarization and the effective anisotropy energy of composite, as a result more and more scattering occurs which leads to the high SE (SE_T~51dB) in comparison to conventional materials. The synthesized in-filled novel micro tubes have better microwave absorption properties (SE_A~43dB) which strongly depends upon optimal infilling of RF in PANI matrix. Additionally, the microwave absorption properties can be tailored easily by varying the PANI/RF ratio and thickness of the samples. Thus, the obtained results suggest that the PANI composite is a new promising microwave absorption material

with vast utility in radio frequency range maintaining strong absorption.

Acknowledgment

The authors wish to thank Prof. R. C. Budhani, Director, NPL, for his keen interest in the work. The authors thank Dr. N. Vijayan, K. N. Sood and Dr. Vidyanand for recording XRD pattern, SEM micrograph and HRTEM, respectively.

Notes and references

[a]*Polymeric & Soft Materials Section, CSIR-National Physical Laboratory, Dr. K. S. Krishnan Road, New Delhi –110 012 (India)*
[b]*Materials Physics and Engineering Division, CSIR-National Physical Laboratory, Dr. K. S. Krishnan Road, New Delhi –110 012 (India)*
[c]*Physics and Engineering of Carbon, CSIR-National Physical Laboratory, Dr. K. S.*
Krishnan Road, New Delhi –110 012 (India)
[d]*Department of Physics & Astrophysics, University of Delhi, Delhi – 110 007 (India)*

** Corresponding author. Tel.: +91-11-45609401, PRFx: +91-11-25726938*
E-mail address: skdhawan@mail.nplindia.ernet.in

‡ Footnotes should appear here. These might include comments relevant to but not central to the matter under discussion, limited experimental and spectral data, and crystallographic data.

† Electronic Supplementary Information (ESI) available: [details of any supplementary information available should be included here]. See DOI: 10.1039/b000000x/

References:

1. G. Tong, W. Wu, Q. Hua, Y. Miao, J. Guan and H. Qian, *Journal of Alloys and Compounds*, 2011, **509**, 451-456.
2. T. GuoXiu, Y. JinHao, M. Ji, Q. M. Yue, G. J. Guo, L. L. Chao, G. PeiJun and C. JianJing, *SCIENTIA SINICA Chimica*, 2011, **41**, 1121-1126.
3. D. D. L. Chung, *Carbon*, 2001, **39**, 279-285.
4. A. P. Singh, M. Mishra, A. Chandra and S. K. Dhawan, *Nanotechnology*, 2011, **22**, 9.
5. M. Mishra, A. P. Singh and S. K. Dhawan, *Journal of Alloys and Compounds*, 2013, **557**, 244-251.
6. A. P. Singh, P. Garg, F. Alam, K. Singh, R. B. Mathur, R. P. Tandon, A. Chandra and S. K. Dhawan, *Carbon*, 2012, **50**, 3868–3875.
7. N. C. Das, D. Khastgir, T. K. Chakia and A. Chakraborty, *Composites Part A: Applied Science and Manufacturing*, 2000, **31**, 1069-1081.
8. S. Yang, K. Lozano, A. Lomeli, H. D. Foltz and R. Jones, *Composites Part A: Applied Science and Manufacturing*, 2005, **36**, 691 -697.
9. L. Li and D. D. L. Chung, *Composites*, 1994, **25**, 215-224.
10. A. P. Singh, B. K. Gupta, M. Mishra, Govind, A. Chandra, R. B. Mathur and S. K. Dhawan, *Carbon*, 2013, **56**, 86–96.
11. K.-Y. Park, J.-H. Han, S.-B. Lee, J.-B. Kim, J.-W. Yi and S.-K. Lee, *Composites Science and Technology*, 2009, **69**, 1271-1278.
12. Y. Huang, N. Li, Y. Ma, F. Du, F. Li, X. He, X. Lin, H. Gao and Y. Chen, *Carbon*, 2007, **45**, 1614-1621.
13. N. Li, Y. Huang, F. Du, X. He, X. Lin, H. Gao, Y. Ma, F. Li, Y. Chen and P. C. Eklund, *Nano Lett*, 2006, **6**, 1141-1145.
14. M. H. Al-Saleh and U.Sundararaj, *Carbon*, 2009, **47** 1738-1746.
15. C.-S. Zhang, Q.-Q. Ni, S.-Y. Fu and K. Kurashiki, *Composites Science and Technology*, 2007, **67**, 2973-2980.
16. B. Belaabed, J. L. Wojkiewicz, S. Lamouri, N. El Kamchi and T. Lasri, *Journal of Alloys and Compounds*, 2012, **527**, 137-144.
17. S. Goswami, U. N. Maiti, S. Maiti, S. Nandy, M. K. Mitra and K. K. Chattopadhyay, *Carbon*, 2011, **49**, 2245-2252.
18. G. Eda and M. Chhowalla, *Nano Lett*, 2009, **9 (2)**, 814-818.
19. X. Fu and D. D. L. Chung, *Cement and Concrete Research*, 1996, **26**, 1467-1472.
20. Y. H. Jianfeng Shen, Min Shi, Na Li, Hongwei Ma and Mingxin Ye, *J. Phys. Chem. C*, 2010, **114 (3)**, 1498-1503.
21. H. He and C. Gao, *Appl. Mater. Interfaces*, 2010, **2 (11)**, 3201-3210.
22. V. Chandra, J. Park, Y. Chun, J. W. Lee, I.-C. Hwang and K. S. Kim, *ACS Nano*, 2010, **4**, 3979-3986.
23. J. Liang, Y. Xu, D. Sui, L. Zhang, Y. Huang, Y. Ma, F. Li and Y. Chen, *J. Phys. Chem. C*, 2010, **114**, 17465-17471.
24. H. Xu, H. Zhang, T. Lv, H. Wei and F. Song, *Colloid Polym Sci*, 2013, **291**, 1713-1720.
25. A. Ohlan, K. Singh, A. Chandra and S. K. Dhawan, *Journal of Applied Polymer Science*, 2008, **108**, 2218-2225.
26. R.-B. Yang, W.-F. Liang, W.-S. Lin, H.-M. Lin, C.-Y. Tsay and C.-K. Lin, *Journal of Applied Physics*, 2011, **109**, -.
27. K. Singh, A. Ohlan, P. Saini and S. K. Dhawan, *Polymers for Advanced Technologies*, 2008, **19**, 229-236.
28. X. Sun, J. He, G. Li, J. Tang, T. Wang, Y. Guo and H. Xue, *Journal of Materials Chemistry C*, 2013, **1**, 765-777.
29. B. H. Kim, D. H. Park, J. Joo, S. G. Yu and S. H. Lee, *Synthetic Metals*, 2005, **150**, 279-284.
30. M. Kanungo, A. Kumar and A. Q. Contractor, *Anal. Chem.*, 2003, **75**, 5673-5679.
31. F. Cheng, W. Tang, C. Li, J. Chen, H. Liu, P. Shen and S. Dou, *Chemistry - A European Journal*, 2006, **12**, 3082 – 3088.
32. X. Lu, H. Mao, D. Chao, W. Zhang and Y. Wei, *Journal of Solid State Chemistry*, 2006, **179**, 2609-2615.
33. A. P. Singh, A. K. S., Amita Chandra and S. K.Dhawan, *AIP ADVANCES*, 2011, **1**, 022147.
34. J. C. Michaelson and A. McEvoy, *J. Chem. Commun.*, 1994, **79**.
35. T. K.Gupta, B. P.Singh, S. R.Dhakate, V. N. Singh and R. B. Mathur, *Journal of Materials Chemistry A*, 2013.
36. S.-H. Shim and T. S. Duffy, *American Mineralogist*, 2002, **87**, 318-326.
37. J. E. P. d. Silva, D. L. A. d. Faria, S. I. C. d. Torresi and M. L. A. Temperini, *Macromolecules*, 2000, **33**, 3077-3083.
38. A. Shakoor, T. Z. Rizvi and A. Nawaz, *J Mater Sci: Mater Electron*, 2011, **22**, 1076-1080.
39. N. F. Colaneri and L. W. Shacklette, *IEEE Trans. Instrum. Meas.*, 1992, **41**, 291-297.
40. A. M. Nicolson and G. F. Ross, *IEEE Trans. Instrum Mea*, 1970, **19** 377−382.
41. A. Ohlan, K. Singh, A. Chandra, V. N. Singh and S. K. Dhawan, *Journal of Applied Physics*, 2009, **106**, 044305-044311.
42. D. L. Leslie-Pelecky and R. D. Rieke, *Chem. Mater.*, 1996, **8**, 1770-1783.
43. Y.-J. Chen, P. Gao, R.-X. Wang, C.-L. Zhu, L.-J. Wang, M.-S. Cao and H.-B. Jin, *J. Phys. Chem. C*, 2009, **113**, 10061–10064.

44. V. K. Sachdev, K. Patel, S. Bhattacharya and R. P. Tandon, *Journal of Applied Polymer Science*, 2011, **120**, 1100-1105.
45. N. C. Das, D. Das, T. K. Khastgir and A. C. Chakrraborthy, *Composites A.*, 2000, **31**, 1069-1081.
46. N. F. Colaneri and L. W. Shacklette, *IEEE Trans. Instrum. Meas.*, 1992, **41**, 29.
47. K. Singh, A. Ohlan, R. K. Kotnala, A. K. Bakhshi and S. K. Dhawan, *Materials Chemistry and Physics*, 2008, **112**, 651-658.
48. Y.-Y. Kim, J. Yun, Y.-S. Lee and H.-I. Kim, *Carbon*, 2011, **12**, 48-52.
49. J. Yun, J. S. Im, H.-I. Kim and Y.-S. Lee, *Colloid Polym Sci.*, 2011, **289**, 1749-1755.
50. K. Singh, A. Ohlan, V. H. Pham, B. R., S. Varshney, J. Jang, S. H. Hur, W. M. Choi, M. Kumar, S. K. Dhawan, B.-S. Kong and J. S. Chung, *Nanoscale*, 2013, **5**, 2411-2420.
51. X. Sun, J. He, G. Li, J. Tang, T. Wang, Y. Guo and H. Xue, *J. Mater. Chem. C*, 2013, **1**, 765-777.